The Moisture Budget of the Polar Atmosphere in MERRA

RICHARD I. CULLATHER
Earth System Science Interdisciplinary Center, University of Maryland, College Park

MICHAEL G. BOSILOVICH
Global Modeling and Assimilation Office,
NASA Goddard Space Flight Center, Greenbelt, Maryland

Submitted to: *Journal of Climate*

Corresponding author address: Richard Cullather, % NASA/GSFC Code 610.1,
8800 Greenbelt Road, Greenbelt, MD 20771.
E-mail: richard.cullather@nasa.gov

ABSTRACT

The atmospheric moisture budget from the Modern Era Retrospective-analysis for Research and Applications (MERRA) is evaluated in polar regions for the period 1979-2005 and compared with previous estimates, accumulation syntheses over polar ice sheets, and in situ Arctic precipitation observations. The system is based on a non-spectral background model and utilizes the incremental analysis update (IAU) scheme. The moisture convergence from MERRA for the north polar cap is comparable to previous estimates using ERA-40 and earlier reanalyses, but is more than 50 percent larger than MERRA $P-E$ computed from physics output fields. This imbalance is comparable to earlier reanalyses for the Arctic. For the south polar cap, the imbalance is 20 percent. The MERRA physics output fields are also found to be overly sensitive to changes in the satellite observing system, particularly over data-sparse regions of the Southern Ocean. Comparisons between MERRA and prognostic fields from two contemporary reanalyses yield a spread of values from 6 percent of the mean over the Antarctic ice sheet to 61 percent over a domain of the Arctic Ocean. These issues highlight continued problems associated with the representation of cold climate physical processes in global data assimilation models. The distribution of MERRA surface fluxes over the major polar ice sheets emphasizes larger values along the coastal escarpments, which agrees more closely with recent assessments of ice sheet accumulation using regional models. Differences between these results and earlier assessments illustrate a continued ambiguity in the surface moisture flux distribution over Greenland and Antarctica.

1. Introduction

The Modern Era Retrospective-analysis for Research and Applications (MERRA) has recently been produced by NASA's Global Modeling and Assimilation Office (GMAO). The objectives of MERRA are to provide a climate context for the NASA satellite observing system and to improve the representation of the water cycle in reanalyses. Numerical reanalyses have been useful in making the historical record more homogeneous and accessible for many applications (Trenberth et al., 2008). For the Arctic and the Antarctic, atmospheric analyses are important tools for the systematic evaluation of large-scale atmospheric phenomena. Reanalysis fields have been widely used in weather and climate studies of the polar regions due to their utility in marshalling the sparse available observations of these areas into a gridded, coherent, and (arguably) plausible dynamical representation of the atmospheric state. Innovative research has been conducted using reanalyses which have led to the recognition of high latitude teleconnection patterns (e.g., Thompson and Wallace, 1998; Hurrell et al., 2001; Genthon et al., 2003; Monaghan and Bromwich, 2008) and the identification of prevailing atmospheric conditions during recent, dramatic reductions in Arctic perennial sea ice cover (Ogi and Wallace, 2007). Reanalyses are also used as first-order validation for climate models and provide necessary boundary forcing conditions for ocean - sea ice, land surface, and limited area atmospheric models (e.g., Walsh et al., 2002; Rinke et al., 2006). Notwithstanding these wide-ranging and constructive applications, reanalyses contain some degree of uncertainty because of the limitations in the observing systems, inconsistencies between differing observations, and incomplete knowledge of the physical processes that are represented in the background weather forecast model (e.g., Thorne, 2008; Grant et al., 2008; Bitz and Fu, 2008; Hines et al., 2000). An initial evaluation of a reanalysis record is therefore a useful undertaking.

The purpose of this study is to provide a basic overview of the quality of MERRA in polar regions. To this end we focus on the atmospheric moisture budget, which has recently been the subject of other studies. A companion paper examines the representation of the atmospheric energy budget in MERRA over high latitudes (Cullather and Bosilovich, 2010). The surface moisture balance in polar regions including the large continental ice sheets and sea ice zones has significant relevance to a wide variety of physical science disciplines with potential importance for understanding eustatic change. Together with the energy balance, these budgets provide an important starting point for evaluating this reanalysis. Some of the questions to be addressed are:

- What are the spatial and temporal patterns of moisture budget components in MERRA, and how do they compare with previous studies?
- How does the MERRA surface moisture flux compare with in situ observations?
- What is the nature of adjustment terms in the budget?

Section 2 provides an overview of the MERRA data set and method. An evaluation of the surface moisture flux in polar regions is provided in section 3. A discussion of these comparisons is then given in section 4.

2. MERRA description and method

The MERRA collection was made using the Data Assimilation System component of the Goddard Earth Observing System (GEOS DAS, Rienecker et al., 2009), and covers the modern satellite era from 1979 to the present. The MERRA time series was produced in three segments as described by Rienecker et al. (2010). The assimilation system utilizes the GEOS model, version 5 (GEOS-5)– a finite-volume atmospheric general circulation model (AGCM) that is used for operational numerical weather prediction. For MERRA, the GEOS DAS was run at a

horizontal resolution of 2/3° longitude by 1/2° latitude and 72 hybrid-sigma coordinate vertical levels to produce an observational analysis at 6-hour intervals. Prescribed conditions include climatological aerosol and solar forcing. Sea surface temperature and sea ice are linearly interpolated in time from weekly 1-degree resolution Reynolds fields (Reynolds, 2002). For the radiative transfer model, a 50 percent sea ice fraction threshold is used to distinguish ice from open water. On non-glaciated land the atmospheric model is coupled to a catchment-based hydrologic model (Koster et al., 2000) and a sophisticated multi-layer snow model (Stieglitz et al., 2001) that is coupled to the catchment hydrology. Land-surface albedos are derived from MODIS retrievals (Moody et al., 2005).

For each analysis, the system incorporates the state of the background forecast model which is taken at the analysis time, at three hours prior, and at three hours after the time, with all the available observations taken over the encompassing six-hour interval to produce gridded fields of state and dynamical variables. The difference between this reference and the background forecast model state is then calculated to produce an analysis tendency (Lucchesi, 2008). The forecast model is then run again over the six hour interval with this tendency added as an additional model forcing term. The output fields of this simulation are preserved at one-hourly intervals. The resulting MERRA product is then composed of dynamically-consistent one-hourly fields that are incrementally corrected to observation every six hours. One advantage of this method– referred to as the incremental analysis update (IAU; Bloom et al., 1996)– is that it explicitly quantifies adjustment terms in atmospheric balance equations. Thus atmospheric budgets– as they are constructed in the GEOS-5 AGCM– and their incremental adjustments are maintained within MERRA to the accuracy limited by round-off and data compression errors. This may be contrasted with alternative systems where a temporal mismatch arises in balance

equations between instantaneous analysis fields and forecast variables that are accumulated over some model integration period. The IAU additionally limits model spin-down as the GEOS DAS progresses over the six hour window and allows for the hourly temporal resolution of output variables.

The atmospheric moisture budget for MERRA may be written as

$$\frac{\partial(W_v + W_l + W_i)}{\partial t} + \nabla \cdot \left\{ \int_{p_{top}}^{p_{sfc}} (q_v + q_l + q_i)\, \tilde{\mathbf{V}}\, \frac{dp}{g} \right\} = E - P + \left. \frac{\partial W_v}{\partial t} \right|_{CHM} + \left. \frac{\partial(W_v + W_l + W_i)}{\partial t} \right|_{FIL} + ANA_{(M)} \tag{1}$$

where

$$W_{(v,l,i)} = \int_{p_{top}}^{p_{sfc}} q_{(v,l,i)} \frac{dp}{g} \tag{2}$$

Here, W_v is column integrated water vapor (precipitable water), W_l is total cloud liquid condensate in the atmospheric column, W_i is total cloud ice condensate in the atmospheric column, q_v is specific humidity, q_l is cloud liquid water mixing ratio, q_i is cloud ice mixing ratio, p_{sfc} is surface pressure, p_{top} is the fixed pressure of the top model level which is 0.01 hPa, $\tilde{\mathbf{V}}$ is the horizontal wind vector, and g is the gravity constant. The symbol E represents the vertical flux of water vapor at the surface, P is total (solid plus liquid) precipitation, and $ANA_{(M)}$ is the tendency resulting from the IAU procedure applied to the moisture budget. The first term on the left-hand-side represents a temporal derivative and is given by the summation of three MERRA variables for each water species denoting contributions from model dynamics, physical parameterizations, and the IAU procedure. The relation between MERRA variables and equation notation is detailed in the appendix. The tendency of precipitable water is negligible for the annual mean but may be significant on monthly time scales depending on the local condition. On

112 the right-hand side, the term denoted by the subscript "*CHM*" represents a parameterized source
113 of water vapor in the middle atmosphere from the model chemistry routine and is small
114 (Lucchesi, 2008). The notation "*FIL*" refers to tendencies associated with the "filling" of
115 spurious negative water, which was found to be negligible in all cases.

116 In atmospheric science, the quantity $P-E$ is sometimes referred to as "net precipitation".
117 Disregarding negligible terms, it may be seen from (1) that two different measures of net
118 precipitation are obtainable from reanalysis collections, which differ by the $ANA_{(M)}$ term. Values
119 obtained from the terms on the left-hand side of (1) are derived from analyses of state and
120 dynamic variables in the atmospheric profile and are referred to as the "aerological method"
121 (e.g., Serreze et al., 2006). The expression is derived from the use of rawinsonde measurements
122 but suffices for the use of reanalyses atmospheric profiles of moisture content and transport in
123 determining convergence in the atmospheric column. The second measure is obtained from the
124 first two terms on the right-hand side, which are individual output products of the assimilating
125 model's physical parameterizations. For clarity this method is referred to here as the physics
126 output. Other studies have used different terminology. Over grounded ice sheets of Greenland
127 and Antarctica, net precipitation may be compared with observed surface accumulation with the
128 knowledge that additional terms including meltwater runoff, blowing snow horizontal transport,
129 and the sublimation of post-precipitated blowing snow may be locally large (e.g., Bintanja, 1998;
130 Box et al., 2006).

131 The approach of this work is to evaluate MERRA against prior studies for large-scale
132 areal averages of the terms in (1) over fixed regions of Greenland and Antarctic conterminous
133 grounded ice sheets, sea ice fields, and a particular focus on the polar caps. Corresponding values
134 are also tabulated for two contemporary reanalyses for comparison: the European Centre for

Medium Range Weather Forecasts (ECMWF) Interim product (ERA-I; Simmons et al., 2007) and the U.S. National Centers for Environmental Prediction (NCEP) Climate Forecast System Reanalysis (CFSR; Saha et al., 2010). The ERA-I was produced at T-255 spectral resolution. Precipitation and evaporation fields are produced from 12-hour forecasts initialized by 4D-Var assimilation. Monthly fields of the ERA-I were obtained from the ECMWF Data Server for the years 1989-2005 at a reduced resolution of 1.5° × 1.5°. The CFSR utilize a coupled atmosphere-ocean model for the initial guess field and an interactive sea ice model and was produced at T-382 spectral resolution. Model variables are produced from 6-hour forecasts. Precipitation and latent heat flux fields were obtained at full resolution from the National Climate Data Center for the period 1979-2005. Evaporation for the CFSR was computed from 6-hour prognostic surface latent heat flux fields using snow cover and sea ice conditions to denote the latent heat of phase transition.

The regions of interest are shown in Fig. 1. Historically, budgets of the polar caps have been defined using the 70° parallels as boundaries that roughly correspond to geographical contrasts between land and ocean and a local maximum in the coverage of the in situ observing network. Boundaries composed of parallels have also served for straightforward comparisons with climate models (e.g., Briegleb and Bromwich, 1998). An Arctic Ocean domain is also utilized to roughly correspond with the recent study of Serreze et al. (2006). Finally, a Southern Ocean fixed domain is determined by the farthest north wintertime sea ice edge. In support of these budget comparisons, the evaluation of near-surface state variables against station observations is also instructive. The results presented are for the period 1979-2005. Surface moisture flux and accumulation are given in water-equivalent units.

3. Surface moisture flux

a. Mean distribution and annual cycle

Principal characteristics of the average surface moisture flux over the Northern Hemisphere polar regions are qualitatively represented in the MERRA averaged moisture convergence field contoured in Fig. 2a, and are composed of modest amounts of annual net precipitation over the Arctic Ocean of between 15 and 30 cm yr^{-1}, smaller amounts over land surfaces in northern Canada and Siberia, and local maxima of 100 to 200 cm yr^{-1} or more over eastern Scandinavia, the Gulf of Alaska, Iceland, and southeastern Greenland. These four areas of maxima are associated with wintertime Atlantic and Pacific storm tracks and lie equatorward of the 70°N parallel. The moisture convergence from MERRA over Greenland reflects a characteristic pattern of largest values in the southeastern coastal region, contours of large values extending along the western coast, and smaller values in the northern region and over the higher elevations of the ice sheet. Annual averaged negative values (divergence) are associated with the northernmost reach of the warm surface Norwegian current as it enters the subpolar gyre near Svalbard. On land, values greater than 30 cm yr^{-1} are located to the east of the Central Siberian Plateau and decrease to less than 15 cm yr^{-1} in eastern Siberia. Spurious negative values are found over lower latitude Asian land surfaces. In general, however, the large-scale patterns for the Arctic are qualitatively similar to compiled climatologies such as the Gorshkov Atlas (Gorshkov, 1983) and more recent assessments using other reanalyses (e.g., Serreze et al., 2006; Bromwich et al., 2001). For example, average fields of the ECMWF 40-year re-analysis (ERA-40; Uppala et al., 2005) similarly indicate the Central Siberian Plateau maxima and annual averaged moisture divergence near Svalbard (Bromwich et al., 2001).

Figure 3a shows the annual cycle of the moisture balance components for the north polar cap domain. Similar to results for earlier reanalyses shown in Bromwich et al. (2000), the annual cycle of atmospheric moisture convergence for the north polar cap in MERRA is dominated by the summer months, with the largest amount of 2.8 cm month^{-1} occurring in July and more consistent amounts of 1.1 to 1.5 cm month^{-1} over the winter period November to May. For the north polar cap, the precipitable water tendency term is significant on the seasonal cycle and results in a one month delay between the maxima in convergence (July) and net precipitation (August). Also shown in Fig. 3a are the separate MERRA precipitation and evaporation curves from physics output. Evaporation is plotted as the negative to show the summation resulting in $P-E$. Evaporation reaches a maximum of 1.9 cm month^{-1} in May that is concurrent with the high latitude melt season, and again becomes as large as 1.6 cm month^{-1} in October with the reintroduction of winter conditions over a large open water fraction persisting from summer. While the overall shape of the physics output $P-E$ time series curve (denoted by bold gray) is generally reflective of precipitation, it is also strongly influenced by the maximum in evaporation in May.

The difference between the aerological and physics output net precipitation curves corresponds to the analysis increment quantity $ANA_{(M)}$. The negative value for $ANA_{(M)}$ indicates the aerological $P-E$ is greater than the physics output value. For the annual average, MERRA physics output $P-E$ values are less than 15 cm yr^{-1} over most of the central Arctic Ocean, Siberia, and central Canada, with spurious negative values over the Mackenzie River basin and small areas of Siberia and Alaska. Both estimates of net precipitation are produced by the GEOS data assimilation system that has been incrementally adjusted to a six-hourly observation-based field. However surface fluxes such as precipitation and evaporation are more heavily dependent

on the physical parameterizations of the model than the aerological field. For the north polar cap, $ANA_{(M)}$ is significant in MERRA and ranges from 0.3 cm month^{-1} in January to 1.1 cm month^{-1} in June. The 1979-2005 average for the analysis increments $ANA_{(M)}$ is 7.3 cm yr^{-1} (1.6 cm yr^{-1} standard deviation from annual values). The agreement between the two time series of $P-E$ in Fig. 3a are comparable to NCEP/NCAR and ERA-15 reanalyses aerological and prognostic curves shown in Bromwich et al. (2000)(NCAR: National Center for Atmospheric Research Reanalyses; Kalnay et al., 1996)(ERA-15: fifteen-year Re-Analyses of the ECMWF; Gibson et al., 1997).

For the Southern Hemisphere polar region, the mean surface moisture flux is strongly influenced by the topographic barrier of the Antarctic Ice Sheet. As shown in Fig. 2b, this results in a strong gradient in the averaged moisture convergence along the East Antarctic coastal escarpment, with large values found in coastal Wilkes Land of greater than 90 cm yr^{-1}. Amounts of greater than 100 cm yr^{-1} are seen in coastal regions of the West Antarctic ice sheet and largest mean values of up to 162 cm yr^{-1} are found along the western coast of the Antarctic Peninsula. Negative contours are confined to the southwestern Ross Sea and offshore of Mac Robertson Land near Mawson Station (68°S, 63°E). The polar desert of the East Antarctic Plateau is indicated by the vast area of the interior ice sheet receiving less than 15 cm yr^{-1}. Qualitatively, this region extends farther north than is found in other studies, but the plateau is devoid of spurious negative values in the long-term average that are found to afflict other data sets (see for example Tietäväinen and Vihmab, 2008). Over the adjacent Southern Ocean, values of up to 82 cm yr^{-1} are located equatorward of Victoria Land, while smaller quantities are found in the eastern Pacific sector, and amounts of less than 30 cm yr^{-1} are found in the southern Weddell Sea. The general features of Fig. 2b are plausible for the Southern Hemisphere. For example,

ERA-40 moisture convergence for the period 1979-2001 similarly indicates large amounts in the Southern Ocean north of Victoria Land and smaller values over the ocean in the South Pacific sector adjacent to West Antarctica (Tietäväinen and Vihma, 2008). For the averaged annual time series, the largest surface moisture flux values over the south polar cap in MERRA occur in winter (Fig. 3b) with a maximum in May of 2.1 cm month^{-1} and a minimum of 0.9 cm month^{-1} in December. Figure 3b indicates a suggestion of the semi-annual oscillation in the aerological $P-E$ with a second maximum of 1.8 cm month^{-1} in September. In contrast to the north polar cap, the precipitable water tendency or storage term on monthly time scales is essentially zero. Evaporation from MERRA physics output is less than 0.2 cm month^{-1} during winter months April to September, but reaches 0.6 cm month^{-1} during summer months, which is half of the precipitation value in December and January.

The area-averaged components of the surface moisture flux for the north polar cap and other regions from MERRA are presented in Table 1 for the time period 1979-2005. As noted previously, the difference for the 70°N–90°N domain of 7.3 cm yr^{-1} between MERRA aerological and physics output estimates is large but comparable to that found by Bromwich et al. (2000) for ERA-15 and NCEP/NCAR reanalyses over the period 1979-1993. Serreze et al. (2006) and Jakobson and Vihma (2009) noted a substantially smaller imbalance in ERA-40 between aerological and prognostic estimates of 1.4 cm yr^{-1} for the period 1979-2001. For the north polar cap, the MERRA aerological $P-E$ (denoted by † in Table 1) is larger than most of the recent estimates tabulated by Bromwich et al. (2000) but is within the standard deviation. Of particular note is Serreze et al. (1995) which did not use reanalyses but rather employed the aerological method using the untreated observations of the rawinsonde network and obtained a value of 16.3 cm yr^{-1}. More recently, Groves and Francis (2002) produced a north polar cap

estimate using satellite-retrieved moisture profiles and NCEP/NCAR reanalysis winds of 15.1 cm yr^{-1} for the period 1979-1998, while Jakobson and Vihma (2010) computed 19.2 cm yr^{-1} using ERA-40 aerological values for the period 1979-2001. Given the interannual variability, MERRA compares reasonably well to these previous estimates.

Also shown in Table 1 are corresponding model output values for the ERA-I and CFSR for the north polar cap over available overlapping years. MERRA net precipitation from physics output is less than the other two reanalyses. Notably, the CFSR prognostic $P-E$ exceeds MERRA physics output by about 80 percent and the MERRA aerological value by 16 percent. Most of this difference is associated with CFSR precipitation, which is larger than MERRA and ERA-I for all months of the year. For February, MERRA and ERA-I both average 2.0 cm $month^{-1}$ over concurrent years 1989-2005, while CFSR averages 2.7 cm $month^{-1}$. For August, the CFSR averages 5.1 cm $month^{-1}$, which compares to 3.8 cm $month^{-1}$ for ERA-I and 3.5 cm $month^{-1}$ for MERRA. Differences between MERRA and ERA-I are associated with evaporation. All three products have a semi-annual cycle in evaporation similar to that shown in Fig. 3a for MERRA, however the phase and amplitude differ among the reanalyses for concurrent years. In particular, CFSR and MERRA place the springtime maximum in May while the ERA-I is consistently one month later, and the CFSR indicate much larger evaporation in October than the other two reanalyses. Average evaporation values for October are 2.3 cm $month^{-1}$ for the CFSR, 1.5 cm $month^{-1}$ for the ERA-I, and 1.6 cm $month^{-1}$ for MERRA.

For the Arctic Ocean domain, Serreze et al. (2006) determined ERA-40 values for the period 1979-2001 of 31.0 cm yr^{-1} for model forecast precipitation and 13.0 cm yr^{-1} for prognostic evaporation, yielding a net precipitation value of 19.0 cm yr^{-1}. These values compare with MERRA estimates of 28.5 cm yr^{-1} for physics output precipitation and 15.0 cm yr^{-1} for

physics output evaporation, yielding 13.5 cm yr^{-1} net precipitation for the comparable Arctic Ocean domain shown in Fig. 1. Thus MERRA precipitation and evaporation estimates from this study and ERA-40 values from Serreze et al. (2006) differ significantly as shown in Table 1. The discrepancy in evaporation is examined further in Cullather and Bosilovich (2010) in the discussion of MERRA energy fluxes. An over-simplified representation of sea ice albedo in MERRA results in large biases in shortwave fluxes in May, which leads to compensation by turbulent energy fluxes. Despite these differences in model-derived values, the aerological estimates of net precipitation are nearly equivalent: 21.0 cm yr^{-1} for ERA-40 versus 21.3 cm yr^{-1} for MERRA. Using satellite-derived moisture estimates, Groves and Francis (2002) determined net precipitation over a similar Arctic domain of 14.5cm yr^{-1}, and tabulated $P-E$ estimates from other sources ranging from 10.5 to 19.5 cm yr^{-1}. These estimates are smaller than both ERA-40 and MERRA aerological values.

A useful source of in situ Arctic Ocean precipitation data is the measurements obtained by Russian ice drifting stations (Colony et al., 1998). These gauge-measured daily observations cover the period 1950-1991 and were obtained from manned stations distributed in the central Arctic that were subject to the movement of drifting ice floes. Daily values have been made available by the National Snow and Ice Data Center (NSIDC). The amounts reported have not been bias corrected for wind-induced undercatch and trace reporting (Yang, 1999). Comparisons have been made to MERRA with nine stations that were functioning during period overlapping with MERRA from 1979 to 1991. The nearest MERRA gridpoint is used for daily comparisons, and MERRA amounts are summed over 24 hourly values. As has been found with previous evaluations with reanalyses, temporal comparisons using daily values are challenging due to the episodic nature of the observations and trace precipitation reporting (Bromwich et al., 2000).

Approximately 40 percent of all ice drifting station reports indicate zero precipitation. In contrast, 56 percent of corresponding MERRA daily values range between 0.1 and 0.5 mm day^{-1} water-equivalent. There is also some ambiguity regarding the time definitions for the station values. Temporal averaging produces some agreement between station observations and MERRA. A representative example is shown in Fig. 6 using a synoptic (7-day) running mean for station NP-30, which was located near the international date line between 74°N and 84°N and reported over a period of 1200 days. The correlation of the two time series shown in Fig. 6 is 0.74. Monthly averages are computed for each station for months of more than 20 observing days, resulting in 119 points for comparison. This averaging indicates an annual MERRA bias of 11 percent. The bias is seasonal and produces MERRA overestimates averaging greater than 60 percent in April-June, but less than 2 percent for other months. Given the gauge biases computed by Yang (1999), the temporal agreement on time scales of greater than a few days is suggested to be reasonable.

Estimates of the surface moisture flux for the south polar cap and Antarctica are given in Table 2. For comparison to the south polar cap $P-E$, Genthon and Krinner (1998) computed values using ERA-15 for the period 1979-1993 of 16.2 cm yr^{-1} and 14.5 cm yr^{-1} for aerological and prognostic methods, respectively, while Tietäväinen and Vihma (2008) determined an aerological value from ERA-40 of 17.4 cm yr^{-1} over the period 1979-2001. MERRA values shown in Table 1 are within this broad range of previous estimates. Additional comparisons are made for the conterminous Antarctic grounded ice sheet domain as shown in Fig. 1. Monaghan et al. (2006) tabulated estimates from previous studies for a base period 1985-2001, as well as their results using a polar version of the MM5 regional model with ERA-40 and NCEP reanalyses forcing on lateral boundaries. Using ERA-40 forcing, Monaghan et al. determined a

318 $P-E$ value of 18.0 cm yr^{-1} with a standard deviation of 0.8 cm yr^{-1}, and presented estimates
319 from other sources ranging from 13.5 to 15.7 cm yr^{-1}. A value of 8.4 cm yr^{-1} is given for the
320 NCEP reanalyses prognostic output but this was discounted by Monaghan et al. due to an
321 unrealistically large quantity for *E*. Corresponding MERRA $P-E$ values for the 1985-2001
322 period are 16.7 cm yr^{-1} for the aerological method and 15.0 cm yr^{-1} from physics output.
323 Also shown in Table 2 are corresponding values for the CFSR and ERA-I for the south
324 polar cap. Similar to the north polar cap, the CFSR prognostic *P*, *E*, and $P-E$ are much larger
325 than for the other two reanalyses, while MERRA and ERA-I principally differ in *E*. The CFSR
326 forecast precipitation exceeds MERRA by 41 percent and ERA-I by 43 percent. Over the
327 averaged annual cycle, these differences are largest in summer. Average precipitation in January
328 for the concurrent period 1989-2005 is 2.0 cm $month^{-1}$ for the CFSR, 1.3 cm $month^{-1}$ for ERA-I
329 and 1.2 cm $month^{-1}$ for MERRA. For evaporation, CFSR is larger than the other two reanalyses
330 throughout the annual cycle, while MERRA evaporation is larger than ERA-I for winter months
331 and less than ERA-I in December and January. As precipitation dominates evaporation over the
332 south polar cap, differences in net precipitation are largely reflective of the differences in *P*.
333 While the CFSR prognostic net precipitation value is much larger than the corresponding value
334 for MERRA physics output, it agrees with the MERRA aerological estimate of 19.4 cm yr^{-1}.
335
336 *b. Analysis increments*
337 The spatial distribution of the variable $ANA_{(M)}$ from MERRA in the Arctic is shown in
338 Fig. 4a. The pattern is complex at lower latitudes with large positive and negative values in close
339 proximity over western Europe. For the Arctic, there is some correlation between the spatial
340 distribution of $ANA_{(M)}$ and the moisture convergence, with larger magnitudes of greater than

(−)12 cm yr^{-1} over the North Pacific storm track and smaller values of 0 to (−)8 cm yr^{-1} in Siberia and central Canada. It may be noted that the location of individual rawinsonde stations may be discerned in Fig. 4a for coastal Greenland by closed contours, where a large-scale negative field of −4 to −8 cm yr^{-1} is embedded with the zero contour line at stations locations.

The annual cycle shown in Fig. 3a and spatial pattern of the analysis increments in Fig. 4a evolve over the 1979-2005 time period. Of particular interest is the introduction of data from the Advanced Microwave Sounding Unit (AMSU) in November 1998, which has a significant global impact on MERRA (Bosilovich et al., 2010). For the north polar cap, the magnitude of $ANA_{(M)}$ becomes notably smaller after the introduction of AMSU. For the years 1979-1997, $ANA_{(M)}$ averages −8.1 cm yr^{-1}. This magnitude is reduced to −4.9 cm yr^{-1} for the years 1999-2005. The impact of these abrupt changes may be seen in the MERRA averages given in Table 1 for years before and after the introduction of AMSU data in 1998. The time periods prior to and after the introduction of AMSU may comprise changes associated with trends or interannual variability. However it is seen in Table 1 that the difference between the MERRA aerological and physics output $P-E$ values has changed between these two time periods: this is the impact of the change in the observing system. As seen in Table 1, this change is principally redistributed to P in the balance equation, which increases by 2.0 cm yr^{-1}, and to a lesser degree to other components of the moisture budget. Coastal Greenland upper-air stations are not evident in the $ANA_{(M)}$ field after 1998.

For the south polar cap as shown in Fig. 3b, the analysis increment $ANA_{(M)}$ is seasonally invariant and is less than 0.3 cm $month^{-1}$, which is approximately 30 percent of the surface moisture flux in December and January and 11 percent in winter months. The spatial distribution of $ANA_{(M)}$ for the Southern Hemisphere, shown in Fig. 4b, is roughly correlated with the patterns

364 of the mean moisture convergence field (Fig. 2b). Figure 4 is contoured at the native spatial
365 resolution of MERRA. East Antarctic coastal upper air stations are readily apparent in the
366 $ANA_{(M)}$ field, with a larger contrast between values at station locations and the neighboring field
367 than is shown for Greenland. For comparison, Tietäväinen and Vihma (2008) determined a
368 budget residual between aerological and prognostic $P-E$ estimates for the Antarctic continent
369 from ERA-40. Tietäväinen and Vihma (2008) indicate a larger residual for ERA-40, including
370 values greater than 20 cm yr^{-1} in coastal areas and the Antarctic Peninsula region, than is shown
371 for $ANA_{(M)}$ in MERRA. As seen in Fig. 4b, the magnitude of the MERRA analysis increments
372 averages less than 8 cm yr^{-1} over most of the Antarctic continent and 12 to 16 cm yr^{-1} adjacent
373 to the Peninsula. Similar to the Northern Hemisphere, there is a marked decrease in the
374 magnitude of $ANA_{(M)}$ after the introduction of AMSU in November 1998. The analysis
375 increment averages −3.7 cm yr^{-1} for the period 1979-1997, but −2.2 cm yr^{-1} for the period 1999-
376 2005. Similar to the north polar cap, this reduction of the analysis increment in the balance
377 equation largely affects P, which increases by 2.2 cm yr^{-1} between the two time periods
378 (Table 2). As with Greenland, closed contours associated with coastal stations in the $ANA_{(M)}$ field
379 become less apparent after 1998.

380 The MERRA analysis increment field denotes differences between analyzed variables
381 and the physical parameterizations of the assimilating GEOS-5 forecast model. These differences
382 are significant in coastal regions of major ice sheets where individual upper air stations are
383 discernible prior to 1998. This indicates disagreement in the assimilation of satellite radiances
384 and/or the climate of the assimilating model first guess field with available rawinsonde data. An
385 area of further interest in this regard is the Southern Ocean region as defined in Fig. 1b. The
386 region lies upstream of Antarctic coastal stations and is essentially devoid of routine in situ

observations (Giovinetto et al., 1997). The time series of net precipitation from aerological and physics output methods is shown in Fig. 5a, with the 1979-2005 mean annual cycle from the aerological method subtracted from both curves. The MERRA physics $P-E$ curve indicates a 40 percent step-function increase in November 1998, from an annual mean of 31.7 cm yr^{-1} to 44.5 cm yr^{-1}, while the aerological value increases only slightly from 44.5 cm yr^{-1} prior to the introduction of AMSU in November 1998 to 45.6 cm yr^{-1} thereafter. The result is a marked decrease in the magnitude of the $ANA_{(M)}$ term for the moisture budget. The difference in the two curves in Fig. 5a is then interpreted as an enhanced sensitivity to the GEOS-5 physical parameterizations as compared to the analysis state and dynamic fields for the Southern Ocean with the introduction of AMSU data. The step change in November 1998 is more substantial at lower latitudes of the Southern Ocean domain and during summer months. As seen in Fig. 5a, the introduction of other sensor data produces less significant changes to the MERRA time series with the exception of the Atmospheric Infrared Sounder (AIRS) in October 2002. The adjustment term changes from an average of -12.8 cm yr^{-1} prior to the introduction of AMSU to -2.2 cm yr^{-1} from November 1998 to September 2002, and then to -0.2 cm yr^{-1} from October 2002 through 2005 after the introduction of AIRS. Transitions associated with changes to the observing system are present in other locations (Bosilovich et al., 2010) and MERRA variables including aerological variables, but not to the extent shown for the Southern Ocean. It is speculated that this is due to the number of in situ observations present in other locations that better constrain the analysis fields. Shown in Figs. 5b and 5c are corresponding time series for the north and south polar caps, respectively, with the 1979-2005 mean annual cycle from the aerological method subtracted from both curves. For the north polar cap, the spring and summer differences between aerological and physics output $P–E$ are apparent as a repeating annual cycle

410 in the physics output anomaly (dark solid curve). After 1998, the magnitude of this difference is
411 reduced over the summer period. The August average of $ANA_{(M)}$ is (–)10.3 cm month^{-1}for the
412 period 1979-1997 and (–)3.8 cm month^{-1} for 1999-2005. For the south polar cap shown in
413 Fig. 5c, it is seen that the two curves more closely overlap after 1998, as suggested by Table 2. It
414 is further speculated that the reduction of $ANA_{(M)}$ with time for various locations indicates a
415 greater compatibility of the assimilating model with the present-day observing system. This is
416 not surprising in view of the operational requirements of the assimilation system.

417 It is of interest to understand whether these changes to the observing system affect other
418 reanalyses. Global averages of *P* and *E* from the CFSR indicate a substantial step function in
419 1998 that has been associated with the introduction of AMSU (Saha et al., 1998). Regionally the
420 impacts are more difficult to discern, particularly given the prominant, global El Niño-Southern
421 Oscillation event in 1998 (Bell et al., 1999). In this initial study, aerological values have not been
422 computed for the CFSR or the ERA-I. For the data sparse Southern Ocean, it may be noted that
423 CFSR forecast evaporation abruptly decreases after 1998, while ERA-I forecast *P* decreases. The
424 average for CFSR *E* is 37.7 cm yr^{-1} for 1989-1997 and 31.6 cm yr^{-1} for 1999-2005, while the
425 ERA-I forecast P is 66.7 cm yr^{-1} for 1989-1997 and 65.1 cm yr^{-1} for the later period. Changes in
426 the interannual variability of *P*, *E*, and $P-E$ from the three reanalyses over the full time series are
427 qualitatively discernible. However, such changes require additional evaluation.
428
429 *c. Greenland and Antarctic ice sheets*
430 For the Greenland Ice Sheet, Table 1 presents MERRA surface moisture flux values
431 averaged over the gridded area shown in Fig. 1 of 1.4×10^6 km^2. This area is defined by locations
432 of greater than 50 percent land ice fraction as defined in MERRA using the Global Land Cover

433 Characterization data set (Loveland et al., 2000). For comparison to MERRA flux components,
434 estimates tabulated by Bromwich et al. (1998) of long-term accumulation synthesized from
435 available observations range from 30.2 to 39.5 cm yr^{-1}, and tabulated studies of precipitation
436 from various sources for the late 20th Century range from 27.6 to 39.1 cm yr^{-1}. Box et al. (2006)
437 used a regional atmospheric model calibrated to glaciological observations to obtain estimates of
438 39.9 cm yr^{-1} (2.1 cm yr^{-1} standard deviation) for precipitation and 3.8 cm yr^{-1} (0.3 cm yr^{-1} s.d.)
439 for evaporation over the period 1988-2004. More recently, Burgess et al. (2010) determined an
440 average accumulation of 33.7 cm yr^{-1} using a high resolution regional model for the period
441 1958-2007 that was calibrated with available core data and coastal meteorological observations
442 to remove complex regional biases. The regional model of Burgess et al. (2010) was forced
443 along lateral boundaries by ERA-40 for the period 1958-2002 and ECMWF operational analyses
444 for the period 2002-2007. Annual fields from the Burgess et al. (2010) study have been obtained
445 and regridded to correspond to MERRA estimates for the years 1979-2005. The corresponding
446 accumulation value for Burgess et al. (2010) is 34.4 cm yr^{-1} and is presented in Table 1. Using
447 these studies, MERRA aerological net precipitation is found to exceed previous Greenland Ice
448 Sheet estimates by a range of 6.4 to 18.3 cm yr^{-1}, with most studies tending towards the former
449 value. Figure 7 presents the average MERRA atmospheric moisture convergence, the
450 accumulation analysis of Burgess et al. (2010), and the difference. Figure 7 emphasizes the
451 disagreement in the high precipitation zones of coastal southern and southeastern Greenland,
452 with differences locally greater than 280 cm yr^{-1} in the southeast. The average spatial
453 distribution of Greenland accumulation determined by Burgess et al. (2010) consists of amounts
454 of less than 18 cm yr^{-1} over the northern interior of the ice sheet, values of up to 73 cm yr^{-1} in
455 western Greenland, and maximum accumulation amounts greater than 270 cm yr^{-1} on the

456 southeastern coast. Average annual moisture convergence from MERRA exceeds 400 cm yr^{-1}
457 for point locations in southeastern Greenland. Though less than MERRA, the accumulation
458 amounts of Burgess et al. (2010) in southeastern Greenland are characterized in the study as
459 being larger than previous estimates.

460 In marked contrast to previous studies, a recent effort using a regional model by Ettema
461 et al. (2009) obtained substantially larger coastal accumulation values. Using the Regional
462 Atmospheric Climate Model version 2 (RACMO2) at high spatial resolution and forced at lateral
463 boundaries by ERA-40 and ECMWF operational analyses, Ettema et al. (2009) found an average
464 for $P-E$ over the Greenland Ice Sheet of 41.9 cm yr^{-1} for the period 1958-2007. This intriguing
465 estimate is comparable to MERRA net precipitation values. Additional in situ measurements in
466 southeastern Greenland would appear essential to resolving differences in these studies.

467 At Summit in central Greenland (72°N, 38°W), MERRA averaged moisture convergence
468 is 19.1 cm yr^{-1} with a standard deviation of 3.2 cm yr^{-1}, which compares with observed
469 accumulation of 22 cm yr^{-1} (Bolzan and Strobel, 1994). A time series of annual values of
470 MERRA net precipitation estimates averaged over the Greenland Ice Sheet are shown in Fig. 8 in
471 comparison to estimates using the data set of Burgess et al. (2010). In comparison to the values
472 derived from Burgess et al. (2010), the correlation is 0.67 for the MERRA aerological time series
473 and 0.57 for the MERRA physics values. It may be seen that the difference between the two
474 MERRA time series and the values of Burgess et al. remain stable over the period 1984-1997
475 and increase after 1997. This change in the bias corresponds with the introduction of AMSU and
476 AIRS satellite data streams, although a transition from ERA-40 to ECMWF operational analyses
477 forcing the Burgess et al. regional model may also be important. Averages over a substantial
478 portion of a limited area model domain are likely to be more representative of the boundary

conditions. As compared to the Southern Ocean domain, the MERRA analysis increments over Greenland do not change abruptly with the introduction of the satellite data streams, but rather decrease more linearly from 4.5 cm yr^{-1} to 2.5 cm yr^{-1}. As shown in Table 1, both MERRA aerological and physics output values increase over the period prior to and after 1998.

Also shown in Table 1 are corresponding values for CFSR and ERA-I reanalyses. The ERA-I fields were obtained from ECMWF at coarse resolution, which restricts the interpretation of the coastal maxima in Greenland. The annual averaged CFSR net precipitation field contains values greater than 210 cm yr^{-1} along the southeastern Greenland coast, and the area averaged net precipitation for the CFSR is comparable to the Ettema et al. (2009) value.

As Monaghan et al. (2008) note, many efforts have been made to produce a long-term validating estimate of Antarctic accumulation but suffer from a sparse surface observational network, remote sensing difficulties, and– where atmospheric models are concerned– incomplete cloud and precipitation microphysics. Recently Arthern et al. (2006) produced a gridded compilation using available surface observations and satellite data, which is shown in Fig. 9a. The field is interpolated to the MERRA grid from an initial resolution of 100 km × 100 km. This compilation differs from prior efforts in using AMSR-E microwave radiance as a background field for interpolation. Differences with prior methods by Vaughan et al. (1999) and Giovinetto and Zwally (2000) emphasize larger coastal values, particularly along the East Antarctic coastal escarpment and along the Bellingshausen Sea coast in West Antarctica. For comparison, Figs. 9c and 9d show the MERRA aerological and physics output $P-E$. While the large scale features are similar, the figures illustrates the higher concentration of large amounts in coastal regions in MERRA as compared to the glaciological estimate. In MERRA, the central Antarctic plateau conveyed by the 5 cm yr^{-1} contour is similar to Arthern et al. (2006) but extends farther

502 northward, as noted previously. Not shown, a difference map indicates MERRA aerological $P-E$
503 is larger than Arthern et al. (2006) accumulation by at least 15 cm yr^{-1} for most coastal areas,
504 and is less than the glaciological synthesis by up to 8 cm yr^{-1} in the regions of central Victoria
505 Land to the west of the Transantarctic Mountains, and for locations at higher elevations in West
506 Antarctica. Locally, MERRA is also less than Arthern et al. by more than 15 cm yr^{-1} along the
507 western side of the Lambert Glacier in East Antarctica, the Elsworth Mountains, and near the
508 highest elevations of the Antarctic Peninsula. These differences correspond to a general view of
509 too much net precipitation along the coast and too little in the interior of the continent in
510 MERRA. These regional differences roughly balance for the continental average as seen in
511 Table 2. Given that accumulation is a long-term average that also includes other losses such as
512 wind-blown snow, the differences with MERRA for the conterminous ice sheet average are
513 likely small.

514 Recently, van de Berg et al. (2006) used the output of RACMO2 calibrated to
515 glaciological observations to determine larger estimates along the Antarctic coast than had been
516 reported previously. As seen in Fig. 9b, the spatial pattern of van de Berg et al. (2006) compares
517 more closely with MERRA aerological $P-E$ than Arthern et al. (2006). The result is entirely
518 analogous to the application to Greenland accumulation by Ettema et al. (2009). Additional
519 measurements and analysis of in situ accumulation estimates for the major ice sheets in coastal
520 and low elevation regions would seem to be necessary to resolve discrepancies between Arthern
521 et al. (2006) and van de Berg et al. (2006).
522

5. Summary and Discussion

MERRA, an atmospheric numerical reanalysis product from NASA GMAO, performs well in representing the high latitude atmospheric moisture budget in comparison to previous studies and two contemporary reanalyses. As seen in Tables 1 and 2, estimates of the average surface moisture flux ($P-E$) from MERRA aerological output for regional averages are comparable to previous studies. For the Arctic, the analysis increments, or the difference between MERRA aerological and physics output methods, are large but comparable to studies using aerological and prognostic forecast methods with earlier ERA-15 and NCEP/NCAR reanalyses. The difference between MERRA aerological and physics output methods over Antarctica is in contrast relatively small. The spatial patterns of this difference produce signatures of upper air station locations in coastal regions of major ice sheets, suggesting disagreements between in situ measurements and satellite or background model values. Comparisons with available physics output fields from two contemporary reanalyses and MERRA indicate a large spread of values. Using the average of the physics output entries for MERRA, CFSR, and ERA-I from Tables 1 and 2, the range of values for individual regions is very large. Over Antarctica and the Greenland Ice Sheet, the range is 6 percent and 14 percent, respectively. But over the Southern Ocean and Arctic Ocean domains, the range 43 percent and 61 percent, respectively. This range highlights continued problems associated with the representation of cold climate physical processes in global data assimilation models, particularly over high latitude oceans (e.g., Bourassa et al., 2010).

Over the large continental ice sheets of Greenland and Antarctica, the reanalysis surface moisture flux compares well to climatologies to the extent that the validating fields are in agreement. For Greenland, the time series of annual MERRA values for $P-E$ correlates with the

546 limited area model study of Burgess et al. (2010). This result and others derived from regional
547 climate models (Ettema et al., 2009; van de Berg et al., 2006) should be tempered by the fact that
548 field averages over large regions of a limited area model domain must necessarily be heavily
549 constrained by the lateral boundary forcing fields, which are numerical analyses. MERRA fields
550 tend to agree more closely with recent studies which place larger moisture flux amounts in close
551 proximity to ice sheet margins and coastlines. Gauge observations over the Arctic basin taken at
552 sub-monthly averages are also found to be correlated with the MERRA precipitation time series.
553 Substantial difficulties with MERRA are apparent. In particular, MERRA is highly
554 sensitive to changes in the satellite observing system, and this is clearly shown over the data-
555 sparse Southern Ocean, where time series analysis is problematic. The introduction of the AMSU
556 data stream into MERRA in November 1998 produces discontinuities in time series of moisture
557 budget components (Bosilovich et al., 2010). Comparisons indicate that these changes are less
558 significant in the aerological values, as suggested by Fig. 5. This change in the observing system
559 is known to afflict other reanalyses globally (Saha et al., 2010). Discontinuities coinciding with
560 the introduction of AMSU in regional time series for the data-sparse Southern Hemisphere high
561 latitudes are apparent but require further evaluation. The difference between MERRA aerological
562 and physics output methods is also maximum for the spring months in the Arctic, and this is
563 likely related to difficulties associated with the surface energy budget and the sea ice albedo
564 during the melt season. The study highlights the use of the $ANA_{(M)}$ field as a utility for
565 identifying changes to the observing system on both temporal and spatial scales, and for
566 identifying deficiencies in physical parameterizations for the polar regions (Cullather and
567 Bosilovich, 2010).

This study also highlights the need for reassessment of the surface mass balance of polar ice sheets in coastal margins, as seen by the curious trend of increasing amounts by successive studies. Measurements in these locations are taken in the presence of steep topography and are within close proximity to strong spatial gradients. Difficulties in obtaining accurate in situ accumulation values are detailed in Eisen et al. (2008) but, as they note, more sampling in coastal regions is required for improvement in continental average assessments. Even with reliable point measurements, comparisons to reanalyses are challenging for these areas due to the variable representation of the coastal escarpment in gridded fields. In MERRA, signatures of upper air stations in the $ANA_{(M)}$ field in these locations indicate disagreements between in situ measurements and satellite or background model estimates of atmospheric variables. The recent studies cited also suggest higher spatial resolution such as that afforded by MERRA is essential for adequately representing the surface moisture flux.

Acknowledgments. ECMWF Interim Re-analyses were obtained from the ECMWF Data Server. The CFSR were obtained from the U.S. National Climate Data Center NOMADS server. Output model fields from Burgess et al. (2010) were obtained from Byrd Polar Research Center, The Ohio State University, Columbus, Ohio. Arctic Ocean Snow and Meteorological Observations from Drifting Stations: 1937, 1950-1991, version 1.0., were obtained from the National Snow and Data Center (NSIDC), University of Colorado at Boulder. Digitized Antarctic accumulation map of Arthern et al. (2006) was obtained from British Antarctic Survey (BAS), Cambridge, United Kingdom. The Antarctic accumulation map of van de Berg et al. (2006) was obtained from Le Brocq et al. (2010). This study was funded by grants from the

NASA Modeling Analysis and Prediction Program (MAP) and the NASA Energy and Water cycle Study (NEWS) to the second author.

APPENDIX

Representation of the Atmospheric Moisture Budget Using MERRA Variables

The following MERRA variables are defined as follows:

DQVDT_DYN	Vertically integrated water vapor tendency for dynamics	kg m^{-2} s^{-1}
DQVDT_PHY	Vertically integrated water vapor tendency for physics	kg m^{-2} s^{-1}
DQVDT_ANA	Vertically integrated water vapor tendency for analysis	kg m^{-2} s^{-1}
DQLDT_DYN	Vertically integrated liquid water tendency for dynamics	kg m^{-2} s^{-1}
DQLDT_PHY	Vertically integrated liquid water tendency for physics	kg m^{-2} s^{-1}
DQLDT_ANA	Vertically integrated liquid water tendency for analysis	kg m^{-2} s^{-1}
DQIDT_DYN	Vertically integrated ice water tendency for dynamics	kg m^{-2} s^{-1}
DQIDT_PHY	Vertically integrated ice water tendency for physics	kg m^{-2} s^{-1}
DQIDT_ANA	Vertically integrated ice water tendency for analysis	kg m^{-2} s^{-1}
EVAP	Surface evaporation	kg m^{-2} s^{-1}
PRECTOT	Total surface precipitation flux	kg m^{-2} s^{-1}
DQVDT_CHM	Vertically integrated water tendency for chemistry	kg m^{-2} s^{-1}
DQVDT_FIL	Artificial “filling” of water vapor	kg m^{-2} s^{-1}
DQLDT_FIL	Artificial “filling” of liquid water	kg m^{-2} s^{-1}
DQIDT_FIL	Artificial “filling” of frozen water	kg m^{-2} s^{-1}

It is noted that a tendency may be expressed as the sum of dynamics, physics, and analysis increment variables denoted by "*_DYN*", "*_PHY*", and "*_ANA*", respectively. For example, the tendency of vertically integrated water vapor (precipitable water) is expressed using MERRA variables as follows.

$$\frac{\partial W_{(v)}}{\partial t} \coloneqq DQVDT\_DYN + DQVDT\_PHY + DQVDT\_ANA \tag{3}$$

For atmospheric moisture, convergence is expressed by the dynamics variables. Equation (1) may then be written using MERRA variables as follows.

$$\begin{aligned}
&(DQVDT_DYN + DQVDT_PHY + DQVDT_ANA \\
&\quad + DQLDT_DYN + DQLDT_PHY + DQLDT_ANA \\
&\quad + DQIDT_DYN + DQIDT_PHY + DQIDT_ANA) \\
&\quad - (DQVDT_DYN + DQLDT_DYN + DQIDT_DYN) \\
&= EVAP - PRECTOT + DQVDT_CHM + \\
&\quad (DQVDT_FIL + DQLDT_FIL + DQIDT_FIL) \\
&\quad + (DQVDT_ANA + DQLDT_ANA + DQIDT_ANA)
\end{aligned} \tag{4}$$

REFERENCES

Arthern, R.J., D.P. Winebrenner, and D.G. Vaughan, 2006: Antarctic snow accumulation mapped using polarization of 4.3-cm wavelength microwave emission. *J. Geophys. Res.*, **111**, D06107, doi:10.1029/2004JD005667.

Bell, G.D., M.S. Halpert, V.E. Kousky, M.E. Gelman, C.F. Ropelewski, A.V. Douglas, and R.C. Schnell, 1999: Climate assessment for 1998. *Bull. Amer. Meteor. Soc.*, **80**, S1-S48.

Bintanja, R., 1998: The contribution of snowdrift sublimation to the surface mass balance of Antarctica. *Ann. Glaciology*, **27**, 251-259.

639 Bitz, C.M., and Q. Fu, 2008: Arctic warming aloft is data set dependent. *Nature*, **455**(7210),
640 E3-E4.
641 Bloom, S., L. Takacs, A. DaSilva, and D. Ledvina, 1996: Data assimilation using incremental
642 analysis updates. *Mon. Wea. Rev.*, **124**, 1256-1271.
643 Bolzan, J.F., and M. Strobel, 1994: Accumulation rate variations around Summit, Greenland, *J.*
644 *Glaciol.*, **40**, 56-66.
645 Bosilovich, M.G., F.R. Robertson, and J. Chen, 2010: Global energy and water budgets in
646 MERRA. *J. Climate* (in preparation).
647 Bourassa, M., S. Gille, C. Bitz, D. Carlson, I. Cerovecki, M. Cronin, W. Drennan, C. Fairall, R.
648 Hoffman, G. Magnusdottir, R. Pinker, I. Renfrew, M. Serreze, K. Speer, L. Talley, and G.
649 Wick, 2010: High-latitude ocean and sea ice surface fluxes: Requirements and challenges for
650 climate research. *Bull. Amer. Meteor. Soc.*, (submitted).
651 Box, J.E., D.H. Bromwich, B.A. Veenhuis, L.-S. Bai, J.C. Stroeve, J.C. Rogers, K. Steffen, T.
652 Haran, and S.-H Wang, 2006: Greenland Ice Sheet surface mass balance variability (1988-
653 2004) from calibrated Polar MM5 output. *J. Climate, 19*, 2783-2800.
654 Briegleb, B.P, and D.H. Bromwich, 1998: Polar climate simulations of the NCAR CCM3. *J.*
655 *Climate*, 11, 1270-1286.
656 Bromwich, D.H., R.I. Cullather, Q.-s. Chen, and B.M. Csathó, 1998: Evaluation of recent
657 precipitation studies for Greenland Ice Sheet. *J. Geophys. Res.*, **103**, 26,007-26024.
658 Bromwich, D.H., R.I. Cullather, and M.C. Serreze, 2000: Reanalyses depictions of the Arctic
659 atmospheric moisture budget. In: *The Freshwater Budget of the Arctic Ocean, NATO Science*
660 *Series 2*, vol. 70, pp. 163-196.
661 Bromwich, D. H., S.-H. Wang, and A. J. Monaghan 2001: ERA-40 representation of the Arctic
662 atmospheric moisture budget. In: *Workshop on Re-analysis, 5-9 November 2001*. ERA-40
663 Project Report Series, No. 3, pp. 287-298.
664 Burgess, E.W., R.R. Forster, J.E. Box, E. Mosley-Thompson, D.H. Bromwich, R.C. Bales, and
665 L.C. Smith, 2010: A spatially calibrated model of annual accumulation rate on the Greenland
666 Ice Sheet (1958-2007). *J. Geophys. Res.*, **115**, F02004, doi:10.1029/2009JF001293.
667 Colony, R., V. Radionov, and F.J. Tanis, 1998: Measurements of precipitation and snow pack at
668 Russian north pole drifting stations. *Polar Record*, **34**, 3-14.
669 Cullather, R.I., and M.G. Bosilovich, 2010: The energy budget of the polar atmosphere in
670 MERRA. *J. Climate*, submitted.
671 Eisen, O., M. Frezzotti, C. Genthon, E. Isaksson, O. Magand, M.R. van den Broeke, D.A. Dixon,
672 A. Ekaykin, P. Holmlund, T. Kameda, L. Karlöf, S. Kaspari, V.Y. Lipenkov, H. Oerter, S.
673 Takahashi, and D.G. Vaughan, 2008: Ground-based measurements of spatial and temporal
674 variability of snow accumulation in East Antarctica. *Rev. Geophys.*, **46**, RG2001,
675 doi:10.1029/2006RG000218.
676 Ettema, J., M.R. van den Broeke, E. van Meijgaard, W.J. van de Berg, J.L. Bamber, J.E. Box,
677 and R.C. Bales, 2009: Higher surface mass balance of the Greenland ice sheet revealed by

high-resolution climate modeling. *Geophys. Res. Lett.*, **36**, L12501, doi:10.1029/2009GL38110.

Genthon, C. and G. Krinner, 1998: Convergence and disposal of energy and moisture on the Antarctic polar cap from ECMWF Reanalyses and Forecasts. *J. Climate*, **11**, 1703-1716.

Genthon, C., G. Krinner, and M. Sacchettini, 2003: Interannual Antarctic tropospheric circulation and precipitation variability. *Climate Dynamics*, **21**, 289-307.

Gibson, J.K., P. Kållberg, S. Uppala, A. Hernandez, A. Nomura, and E. Serrano, 1997: *ERA Description*. ECMWF Reanalyis Project Report Series, No. 1, 72 pp.

Giovinetto, M.B., and H.J. Zwally, 2000: Spatial distribution of net surface accumulation on the Antarctic ice sheet. *Ann. Glaciol.*, **31**, 171-178.

Giovinetto, M.B., D.H. Bromwich, and G. Wendler, 1992: Atmospheric net transport of water vapor and latent heat across 70°S. *J. Geophys. Res.*, **97**, 917–930.

Gorshkov, S.G., Ed., 1983: *Arctic Ocean. World Ocean Atlas, Vol. 3*. Pergamon Press, 189 pp.

Grant, A.N., S. Brönnimann, and L. Haimberger, 2008: Recent Arctic warming vertical structure contested. *Nature*, **455**(7210), E2-E3.

Groves, D.G., and J.A. Francis, 2002: Moisture budget of the Arctic atmosphere from TOVS satellite data. J. Geophys. Res., **107**, 4391, doi:10.1029/2001JD001191.

Hines, K.M., D.H. Bromwich, and G.J. Marshall, 2000: Artificial surface pressure trends in the NCEP-NCAR reanalysis over the Southern Ocean and Antarctica. *J. Climate*, **13**, 3940-3952.

Hurrell, J.W., Y. Kushnir, G. Ottersen, and M. Visbeck, 2001: An overview of the North Atlantic Oscillation. *The North Atlantic Oscillation: Climatic Significance and Environmental Impact.* J.W. Hurrell, Y. Kushnir, G. Ottersen, and M. Visbeck, eds., pp. 1-35.

Jakobson, E., and T. Vihma, 2010: Atmospheric moisture budget in the Arctic based on the ERA-40 reanalysis. *Int. J. Climatol.*, in press.

Kalnay, E., M. Kanamitsu, R. Kistler, W. Collins, D. Deaven, L. Gandin, M. Iredell, S. Saha, G. White, J. Woollen, Y. Zhu, A. Leetmaa, R. Reynolds, M. Chelliah, W. Ebisuzaki, W.Higgins, J. Janowiak, K. C. Mo, C. Ropelewski, J. Wang, R. Jenne, and D. Joseph, 1996: The NCEP/NCAR 40-Year Reanalysis Project. *Bull. Amer. Meteorol. Soc.*, **77**, 437-472.

Koster, R.D., M.J. Suárez, A. Ducharne, M. Stieglitz, and P. Kumar, 2000: A catchment-based approach to modeling land surface processes in a GCM, Part 1, Model Structure. *J. Geophys. Res.*, **105**, 24809-24822.

Le Brocq, A.M., A.J. Payne, and A. Vieli, Andreas, 2010: Antarctic dataset in netCDF format. *Publishing Network for Geoscientific & Environmental Data*, doi:10.1594/PANGAEA.734145.

Loveland, T.R., B.C. Reed, J.F. Brown, D.O. Ohlen, Z. Zhu, L. Yang, and J.W. Merchant, 2000: Development of a global land cover characteristics database and IGBP DISCover from 1 km AVHRR data. *Int. J. Remote Sensing*, **21**, 1303-1330.

Lucchesi, R., 2008: *File Specification for MERRA Gridded Output*. Version 2.1. Global Modeling and Assimilation Office, National Aeronautics and Space Administration, Greenbelt, MD., 96 pp.

718 Monaghan, A.J., and D.H. Bromwich, 2008: Advances in describing recent Antarctic climate
719 variability. *Bull. Amer. Meteorol. Soc.*, **89**, 1295-1306.
720 Moody, E.G., M.D. King, S. Platnick, C.B. Schaaf, and F. Gao, 2005: Spatially complete global
721 spectral surface albedos: Value-added datasets derived from Terra MODIS land products.
722 *IEEE Trans. Geosci. Remote Sens.*, **43**, 144–158.
723 Ogi, M., and J.M. Wallace, 2007: Summer minimum Arctic sea ice extent and the associated
724 summer atmospheric circulation. *Geophys. Res. Lett.*, **34**, L12705,
725 doi:10.1029/2007GL029897.
726 Reynolds, R.W., N.A. Rayner, T.M. Smith, D.C. Stokes, and W. Wang, 2002: An improved in
727 situ and satellite SST analysis for climate. *J. Climate*, **15**, 1609–1625.
728 Rienecker, M.M., M.J. Suarez, R. Todling, J. Bacmeister, L. Takacs, H.-C. Liu, W. Gu, M.
729 Sienkiewicz, R.D. Koster, R. Gelaro, I. Stajner, and E. Nielsen, 2009: *The GEOS-5 Data*
730 *Assimilation System- Documentation of Versions 5.0.1, 5.1.0, and 5.2.0*. Technical Report
731 Series on Global Modeling and Data Assimilation, NASA/TM-2007-104606, M.J. Suarez,
732 Ed., Vol. 27, 95 pp.
733 Rienecker M.M., and coauthors, 2010: The NASA Modern Era Retrospective-Analysis for
734 Research and Applications (MERRA). *J. Climate* (in preparation).
735 Rinke, A., K. Dethloff, J.J. Cassano, J.H. Christensen, J.A. Curry, P. Du, E. Girard,
736 J.-E. Haugen, D. Jacob, C.G. Jones, M. Køltzow, R. Laprise, A.H. Lynch, S. Pfeifer,
737 M.C. Serreze, M.J. Shaw, M. Tjernström, K. Wyser, and M. Žagar, 2006: Evaluation of an
738 ensemble of Arctic regional climate models. Spatiotemporal fields during the SHEBA year.
739 *Climate Dynamics*, **26**, 459-472.
740 Saha, S., S. Moorthi, H.-L. Pan, X. Wu, J. Wang, S. Nadiga, P. Tripp, R. Kistler, J. Woollen, D.
741 Behringer, H. Liu, D. Stokes, R. Grumbine, G. Gayno, J. Wang, Y.-T. Hou, H. Chuang, H.H.
742 Juang, J. Sela, M. Iredell, R. Treadon, D. Kleist, P. Van Delst, D. Keyser, J. Derber, M. Ek, J.
743 Meng, H. Wei, R. Yang, S. Lord, H. van den Dool, A. Kumar, W. Wang, C. Long, M.
744 Chelliah, Y. Xue, B. Huang, J.-K. Schemm, W. Ebisuzaki, R. Lin, P. Xie, M. Chen, S. Zhou,
745 W. Higgins, C.-Z. Zou, Q. Liu, Y. Chen, Y. Han, L. Cucurull, R.W. Reynolds, G. Rutledge,
746 and M. Goldberg, 2010: The NCEP Climate Forecast System Reanalysis. *Bull. Amer. Meteor.*
747 *Soc.*, **91**, 1015-1057.
748 Serreze, M.C., R.G. Barry, and J.E. Walsh, 1995: Atmospheric water vapor characteristics at
749 70°N. *J. Climate*, **8**, 719-731.
750 Serreze, M.C., A.P. Barrett, A.G. Slater, R.A. Woodgate, K. Aagaard, R.B. Lammers, M. Steele,
751 R. Moritz, M. Meredith, and C.M. Lee, 2006: The large-scale freshwater cycle of the Arctic.
752 *J. Geophys. Res.*, **111**, C11010, doi:10.1029/2005JC003424.
753 Simmons, A.J., S. Uppala, D. Dee, and S. Kobayashi, 2007: ERAInterim: New ECMWF
754 reanalysis products from 1989 onwards. *ECMWF Newsletter*, **110**, 25–35.
755 Stieglitz, M., A. Ducharne, R.D. Koster, and M.J. Suarez, 2001: The impact of detailed snow
756 physics on the simulation of snow cover and subsurface thermodynamics at continental scales.
757 *J. Hydrometeorol.*, **2**, 228-242.

Thompson, D.W.J., and J.M. Wallace, 1998: The Arctic Oscillation signature in the wintertime geopotential height and temperature fields. *Geophys. Res. Lett.*, **25**, 1297-1300.

Thorne, P.W., 2008: Arctic tropospheric warming amplification? *Nature*, **455**(7210), E1-E2.

Tietäväinen, H., and T. Vihma, 2008: Atmospheric moisture budget over Antarctica and the Southern Ocean based on the ERA-40 reanalysis. *Int. J. Climatology*, **28**, 1977-1995.

Trenberth, K.E., T. Koike, and K. Onogi, 2008: Progress and prospects for reanalysis for weather and climate. *Eos, Trans. Amer. Geophys. Union*, **89**, 234-235.

Uppala, S.M., P.W. Kållberg, A.J. Simmons, U. Andrae, V. da Costa Bechtold, M. Fiorino, J.K. Gibson, J. Haseler, A. Hernandez, G.A. Kelly, X. Li, K. Onogi, S. Saarinen, N. Sokka, R.P. Allan, E. Andersson, K. Arpe, M.A. Balmaseda, A.C.M. Beljaars, L. van de Berg, J. Bidlot, N. Bormann, S. Caires, F. Chevallier, A. Dethof, M. Dragosavac, M. Fisher, M. Fuentes, S. Hagemann, E. Hólm, B.J. Hoskins, L. Isaksen, P.A.E.M. Janssen, R. Jenne, A.P. McNally, J.-F. Mahfouf, J.-J. Morcrette, N.A. Rayner, R.W. Saunders, P. Simon, A. Sterl, K.E. Trenberth, A. Untch, D. Vasiljevic, P. Viterbo, and J. Woollen, 2005: The ERA-40 re-analysis. *Quart. J. R. Meteorol. Soc.*, **131**, 2961-3012.

van de Berg, W.J., M.R. van den Broeke, C.H. Reijmer, and E. van Meijgaard, 2006: Reassessment of the Antarctic surface mass balance using calibrated output of a regional atmospheric climate model. *J. Geophys. Res.*, **111**, D11104, doi:10.1029/2005JD006495.

Vaughan, D.G., J.L. Bamber, M. Giovinetto, J. Russell, and A. P. R. Cooper, 1999: Reassessment of net surface mass balance in Antarctica. *J. Climate*, **12**, 933–946.

Walsh, J.E., V.M. Kattsov, W.L. Chapman, V. Govorkova, and T. Pavlova, 2002: Comparison of Arctic climate simulations by uncoupled and coupled global models. *J. Climate*, **15**, 1429-1446.

Yang, D., 1999: An improved precipitation climatology for the Arctic Ocean. *Geophys. Res. Lett.*, **26**, 1625-1628.

TABLE 1. MERRA average surface moisture flux components for Northern Hemisphere polar regions in comparison to previous results. The standard deviation of annual values is shown in parentheses.

[cm yr^{-1}]	Source	Period	P	E	$P-E$*	$P-E^{\dagger}$
70°N − 90°N (north polar cap)	MERRA	1979-2005	29.9(1.6)	16.7(0.7)	13.2(1.6)	20.5(1.5)
	MERRA	1979-1997	29.5(1.3)	16.8(0.8)	12.8(1.3)	20.9(1.5)
	MERRA	1999-2005	31.5(1.1)	16.6(0.4)	14.8(1.0)	19.8(1.1)
	CFSR	1979-2005	42.3(1.9)	18.6(0.8)	23.7(1.6)	
	ERA-I	1989-2005	31.5(1.4)	13.4(0.9)	18.1(1.5)	
	Bromwich et al.	1979-1993				18.9(2.3)
	Jakobson and Vihma	1979-2001	32.3(2.3)	14.4(0.9)	17.9(2.0)	19.2(1.6)
	Groves and Francis	1979-1998				15.1
	Serreze et al. 1995	1974-1991				16.3
Arctic Ocean	MERRA	1979-2005	28.5(1.7)	15.0(0.8)	13.5(1.7)	21.3(1.7)
	MERRA	1979-1997	28.3(1.5)	15.1(0.8)	13.1(1.5)	21.8(1.6)
	MERRA	1999-2005	29.7(1.5)	14.8(0.6)	14.9(1.2)	20.2(1.5)
	CFSR	1979-2005	41.3(2.3)	17.1(1.0)	24.2(2.1)	
	ERA-I	1989-2005	30.1(1.9)	12.0(1.1)	18.1(1.8)	
	Serreze et al. 2006	1979-2001	31.0	13.0	19.0	21.0(2.1)
Greenland Ice Sheet	MERRA	1979-2005	43.4(4.6)	0.9(0.2)	42.4(4.7)	45.9(4.4)
	MERRA	1979-1997	41.9(4.5)	1.0(0.1)	41.0(4.5)	44.8(4.4)
	MERRA	1999-2005	47.4(2.2)	0.6(0.1)	46.8(2.2)	49.6(1.8)
	CFSR	1979-2005	49.3(4.2)	7.8(0.6)	41.5(4.0)	
	ERA-I	1989-2005	38.7(3.1)	2.0(0.2)	36.7(3.3)	
	Burgess et al.	1979-2005			34.4(2.3)	
	Ettema et al.	1958-2007	43.4(2.3)	1.5	41.9	

* Computed using physics output fields.

† Computed using aerological method.

TABLE 2. MERRA average surface moisture flux components for Southern Hemisphere polar regions in comparison to previous results. The standard deviation of annual values is shown in parentheses.

[cm yr^{-1}]	Source	Period	P	E	$P-E$*	$P-E$†
70°S − 90°S	MERRA	1979-2005	19.8(1.4)	4.3(0.2)	15.5(1.3)	18.8(1.1)
(south polar	MERRA	1979-1997	19.2(0.9)	4.3(0.1)	14.9(0.9)	18.7(1.1)
cap)	MERRA	1999-2005	21.5(1.2)	4.3(0.3)	17.1(1.0)	19.4(1.1)
	CFSR	1979-2005	28.0(0.9)	8.6(0.9)	19.4(1.2)	
	ERA-I	1989-2005	19.6(0.9)	4.0(0.2)	15.7(0.8)	
	Genthon and Krinner	1979-1993				16.2
Antarctic	MERRA	1979-2005	16.5(1.0)	1.1(0.1)	15.4(1.1)	17.1(1.1)
Ice Sheet	MERRA	1979-1997	16.1(0.8)	1.1(0.09)	15.0(0.8)	16.8(1.0)
	MERRA	1999-2005	17.5(1.1)	1.1(0.05)	16.4(1.1)	17.8(1.0)
	CFSR	1979-2005	19.7(0.9)	3.8(0.2)	15.9(0.9)	
	ERA-I	1989-2005	14.2(0.8)	1.7(0.1)	12.5(0.8)	
	Monaghan et al.	1985-2001	20.0		18.0(0.8)	
	Arthern et al.	Long-term				14.3(0.4)‡
	van de Berg et al.	1980-2004				17.1(0.3)‡
Southern Ocean	MERRA	1979-2005	61.8(5.9)	26.7(0.6)	35.1(6.2)	44.9(1.8)
	MERRA	1979-1997	58.7(1.9)	26.9(0.5)	31.8(2.1)	44.7(1.9)
	MERRA	1999-2005	70.8(3.5)	26.2(0.3)	44.6(3.5)	45.7(1.7)
	CFSR	1979-2005	89.7(2.6)	35.5(2.7)	54.1(3.3)	
	ERA-I	1989-2005	66.2(1.7)	23.8(0.6)	42.3(1.7)	

* Computed using physics output fields.

† Computed using aerological method.

‡ Accumulation.

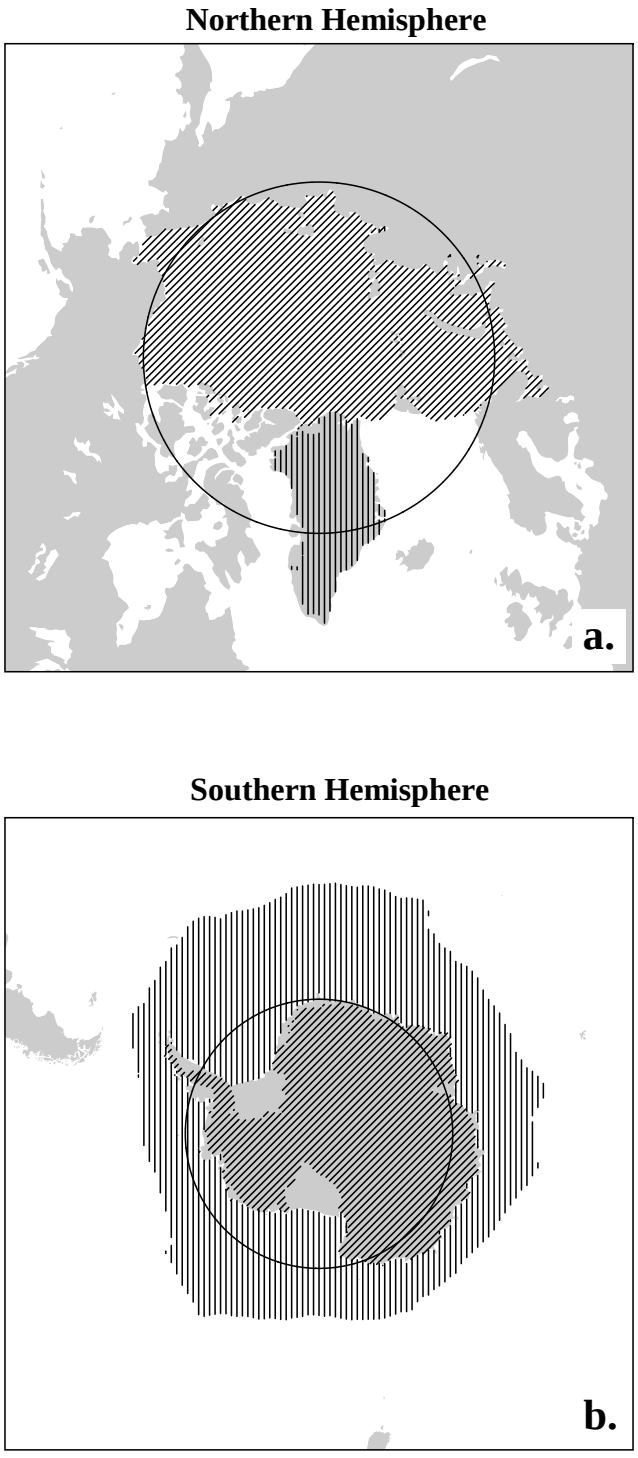

FIGURE 1. Regions of study for (a.) the Northern Hemisphere and (b.) the Southern Hemisphere. Bold line indicates the 70° parallel. Continental areas, which include major ice shelves in Antarctica, are shaded gray.

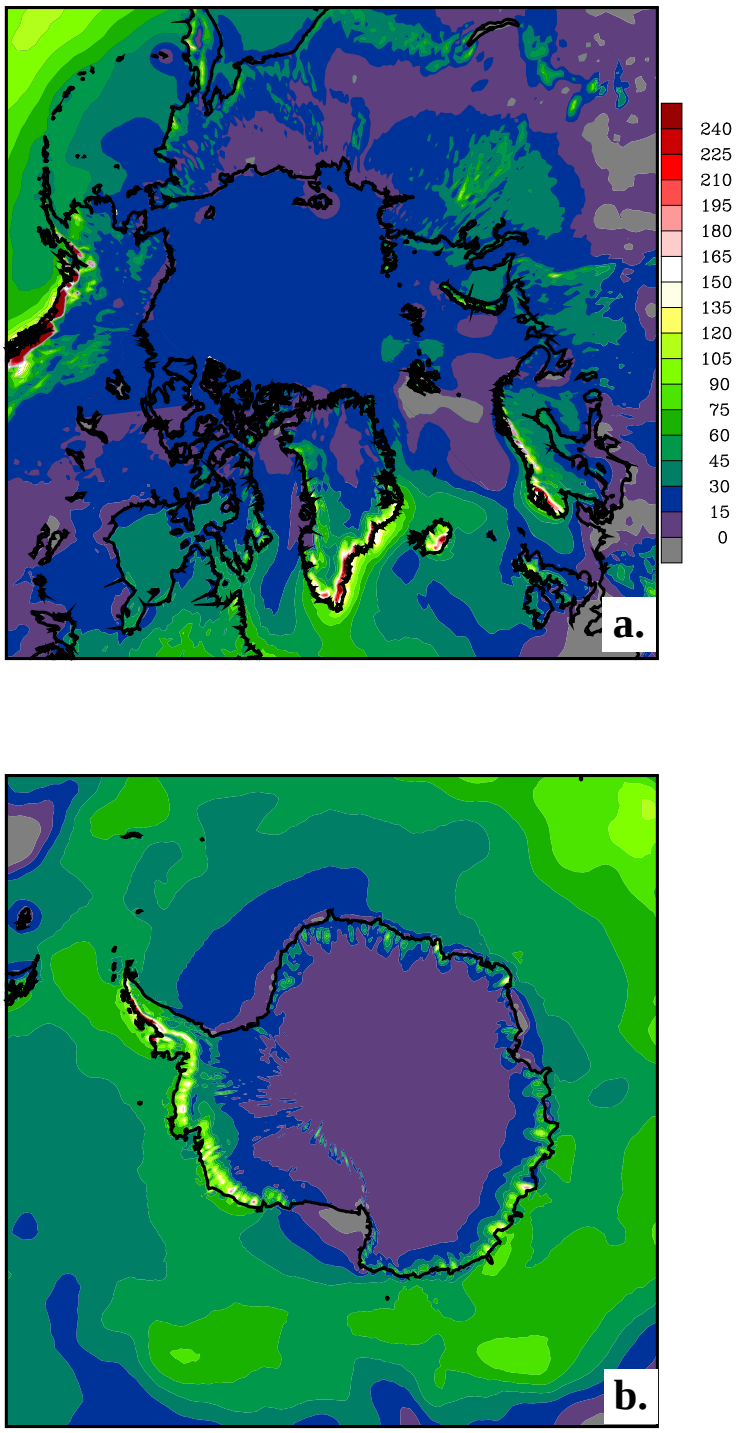

FIGURE 2. Contours of 1979-2005 MERRA atmospheric moisture convergence for high latitudes for (a.) the Northern Hemisphere and (b.) the Southern Hemisphere. The contour interval is 15 cm yr^{-1}.

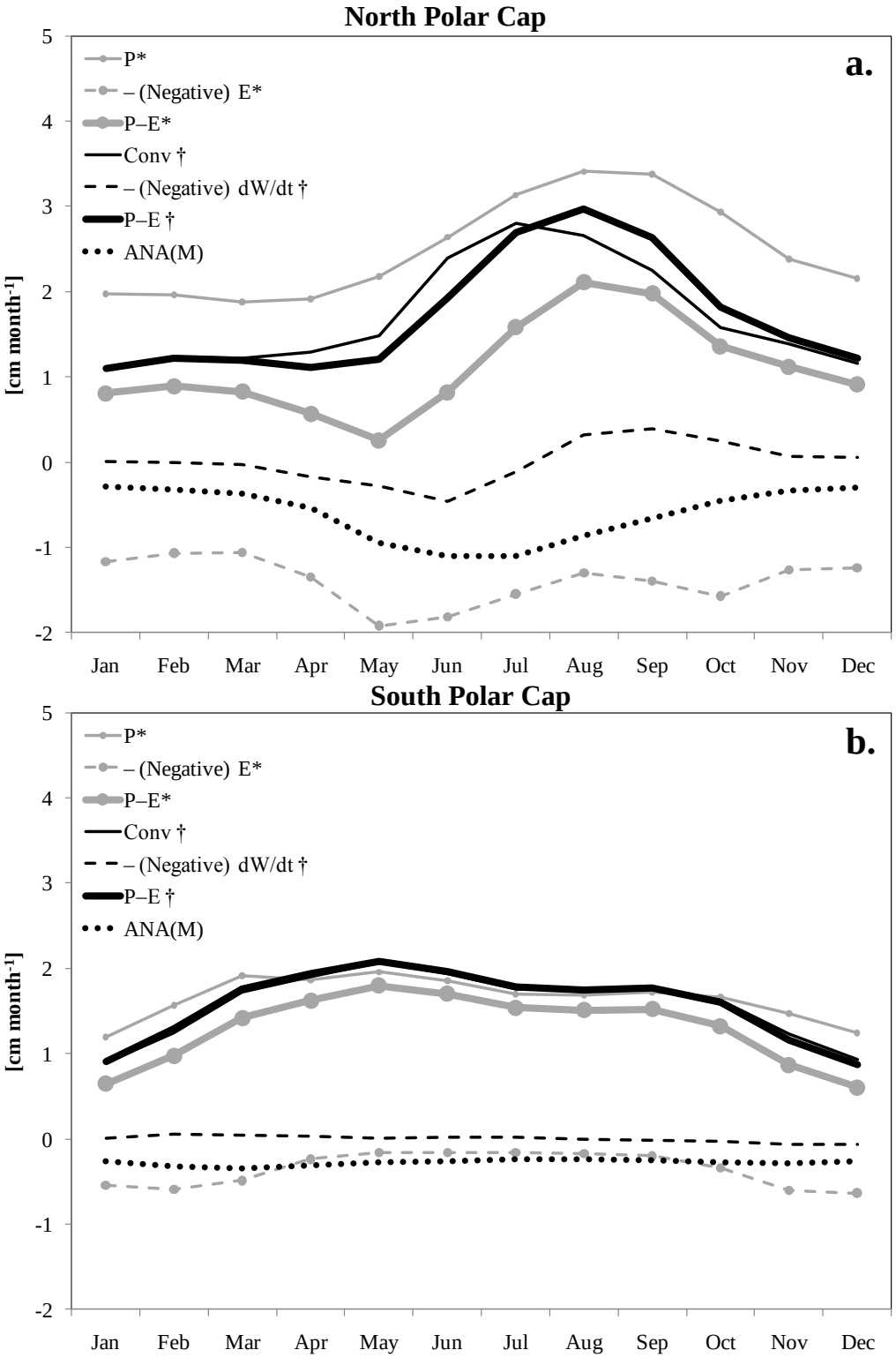

FIGURE 3. Average annual time series for MERRA surface moisture flux components, in cm month^{-1}, for (a.) the north polar cap and (b.) the south polar cap. Values using aerological analysis fields are denoted by †, while physics output fields are denoted by *.

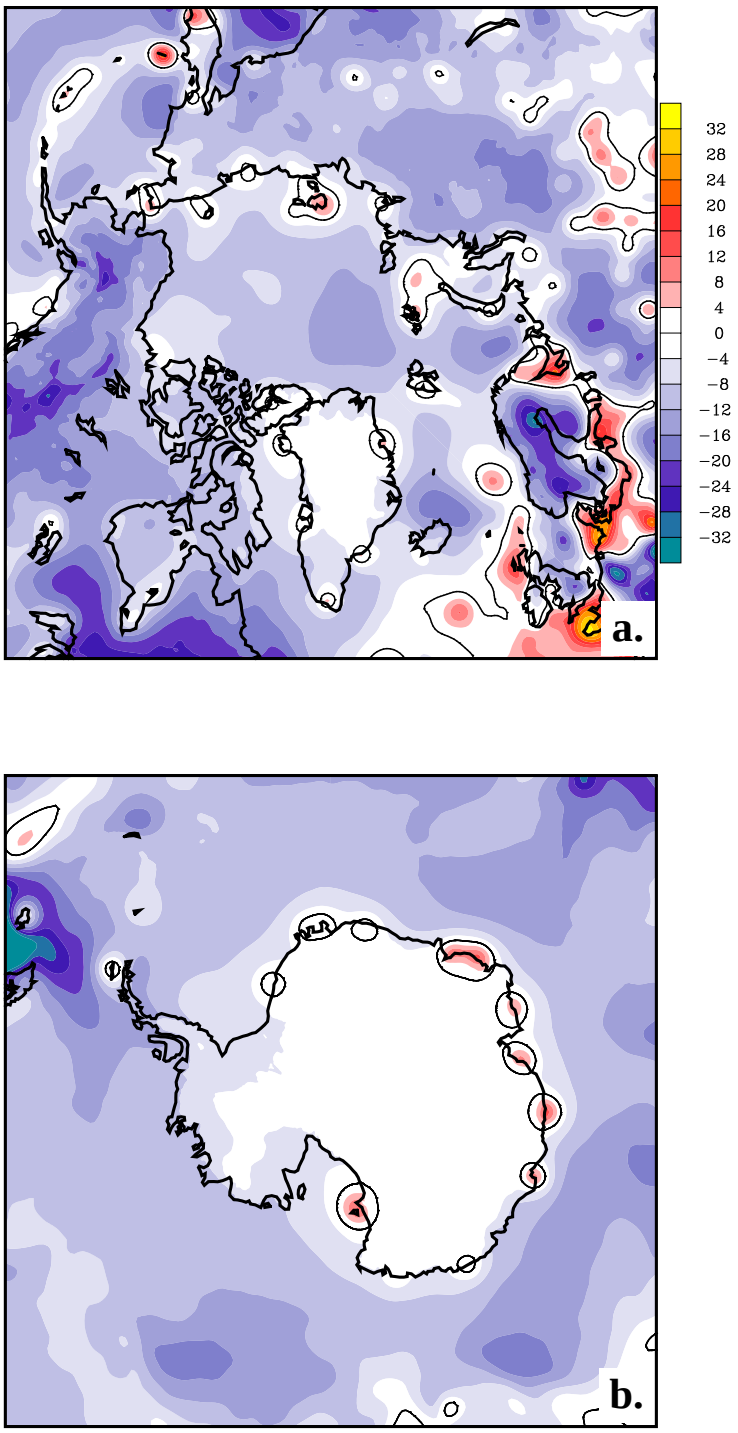

FIGURE 4. Contours of 1979-2005 average MERRA analysis increments field for the surface moisture balance for (a.) the Northern Hemisphere and (b.) the Southern Hemisphere. The contour interval is 4 cm yr^{-1}. The zero contour is indicated as a solid black line.

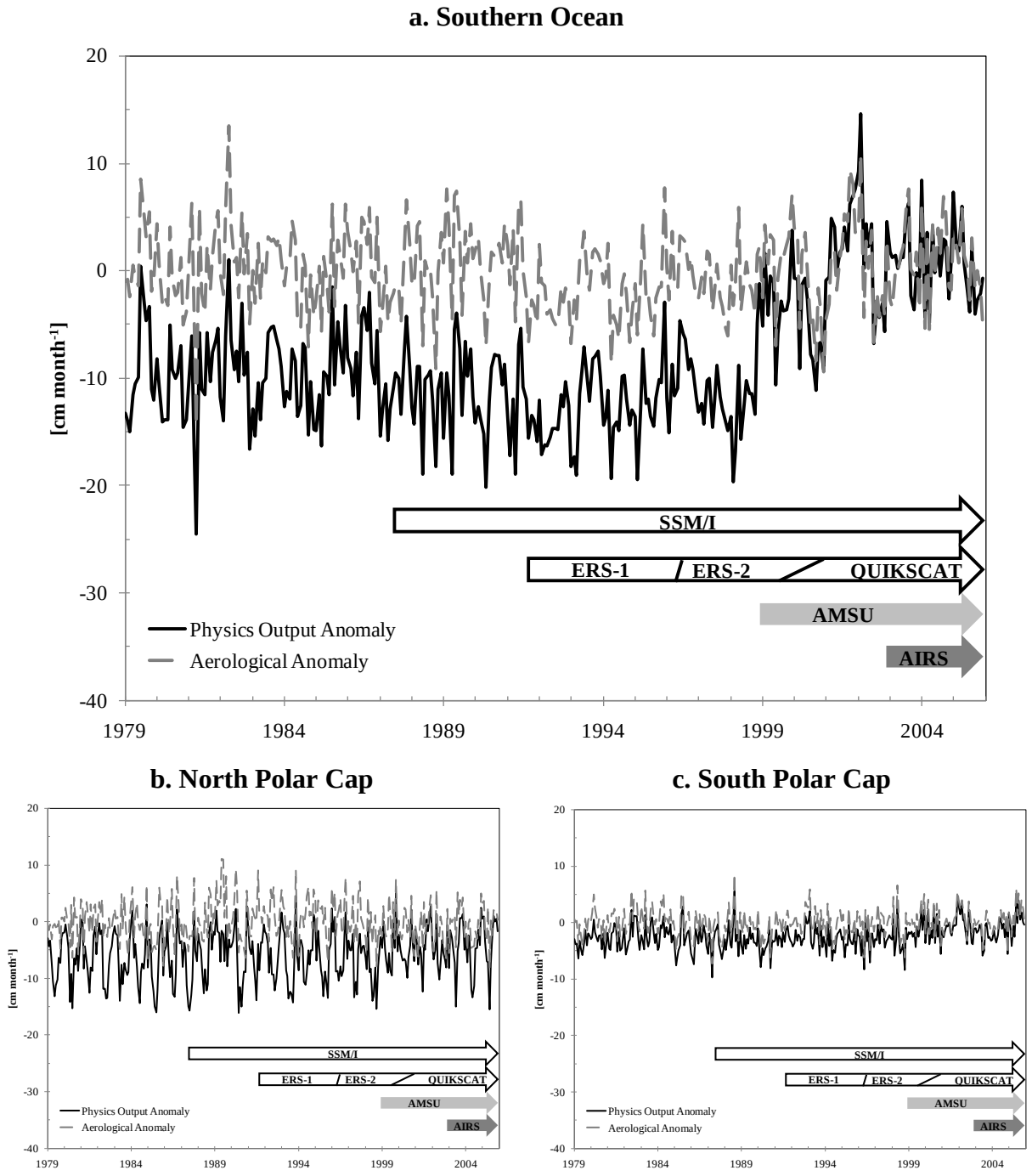

FIGURE 5. MERRA net precipitation monthly anomaly for (a.) the Southern Ocean domain, (b.) the north polar cap, and (c.) the south polar cap based on physics output fields (solid line) and the aerological method (dashed), in cm month^{-1}. The anomaly for each curve is referenced to the aerological method for the period 1979-2005. Arrows indicate the timing of input data for select instruments is shown. The times correspond to the introduction of input data to the assimilation system, which may differ from the time of satellite deployment.

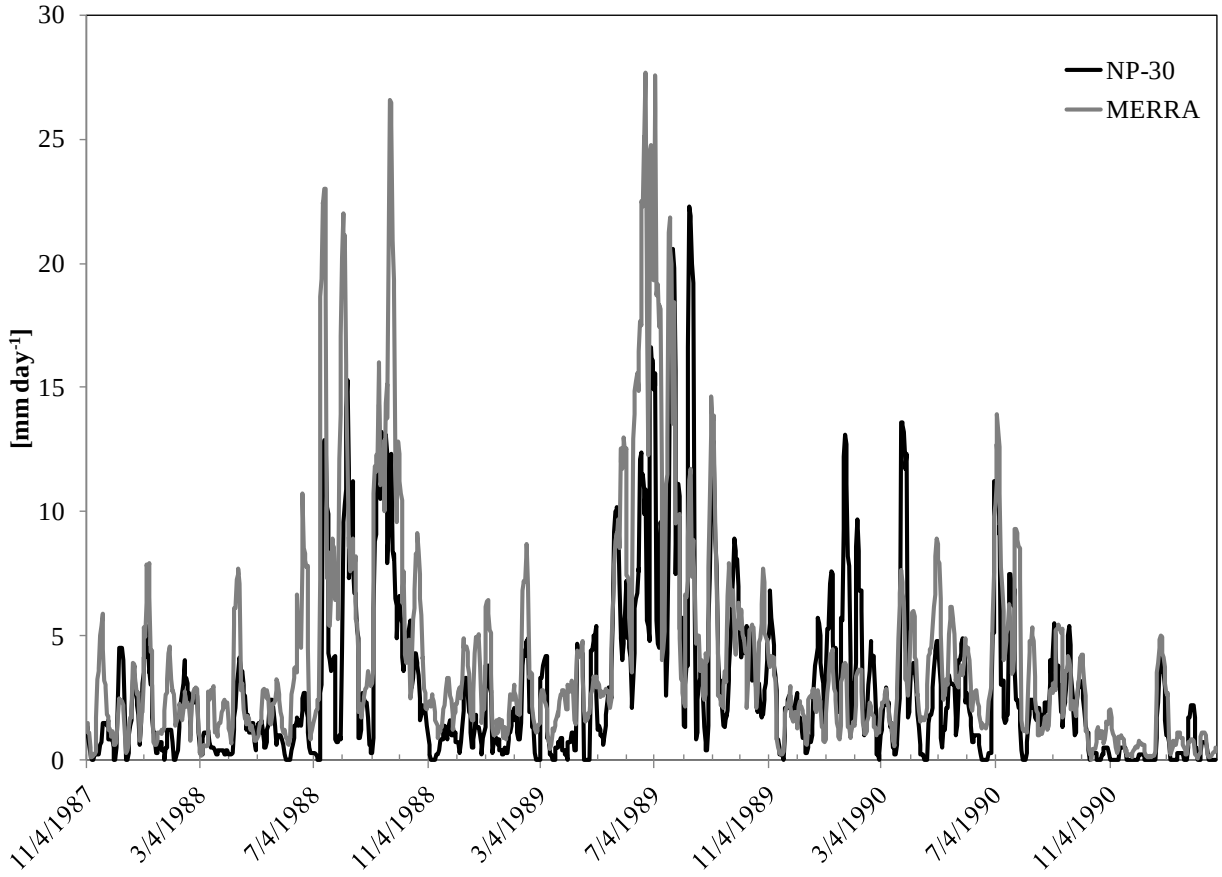

FIGURE 6. Comparison of MERRA with NP-30 Arctic drifting station daily gauge precipitation for a seven day running mean, in mm day^{-1}.

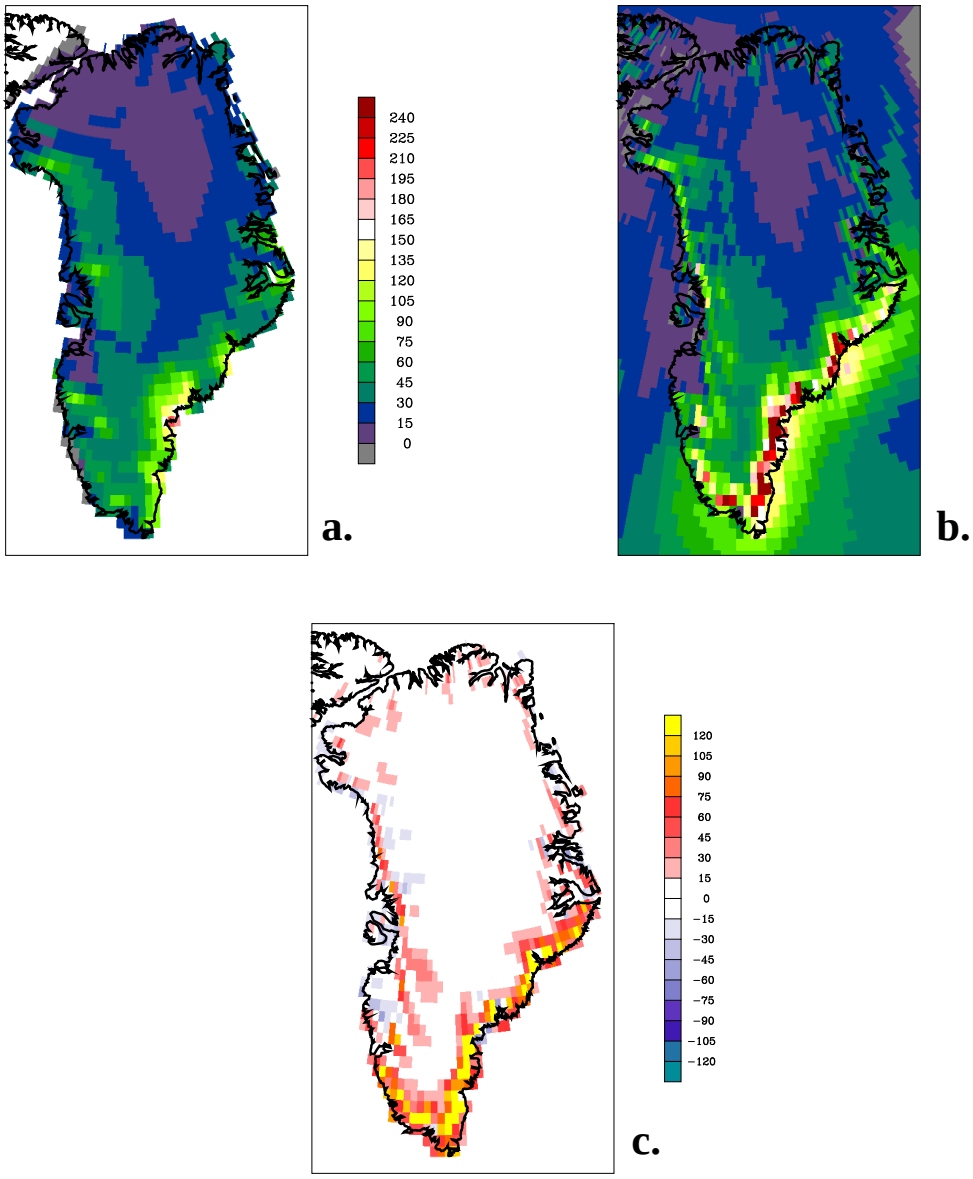

FIGURE 7. Grid cell shading of (a.) Greenland mesoscale model analysis from Burgess et al. (2010) interpolated to the MERRA grid, (b.) MERRA atmospheric moisture convergence, and (c.) MERRA moisture convergence minus Burgess et al. analysis. The shading interval is every 15 cm yr^{-1}.

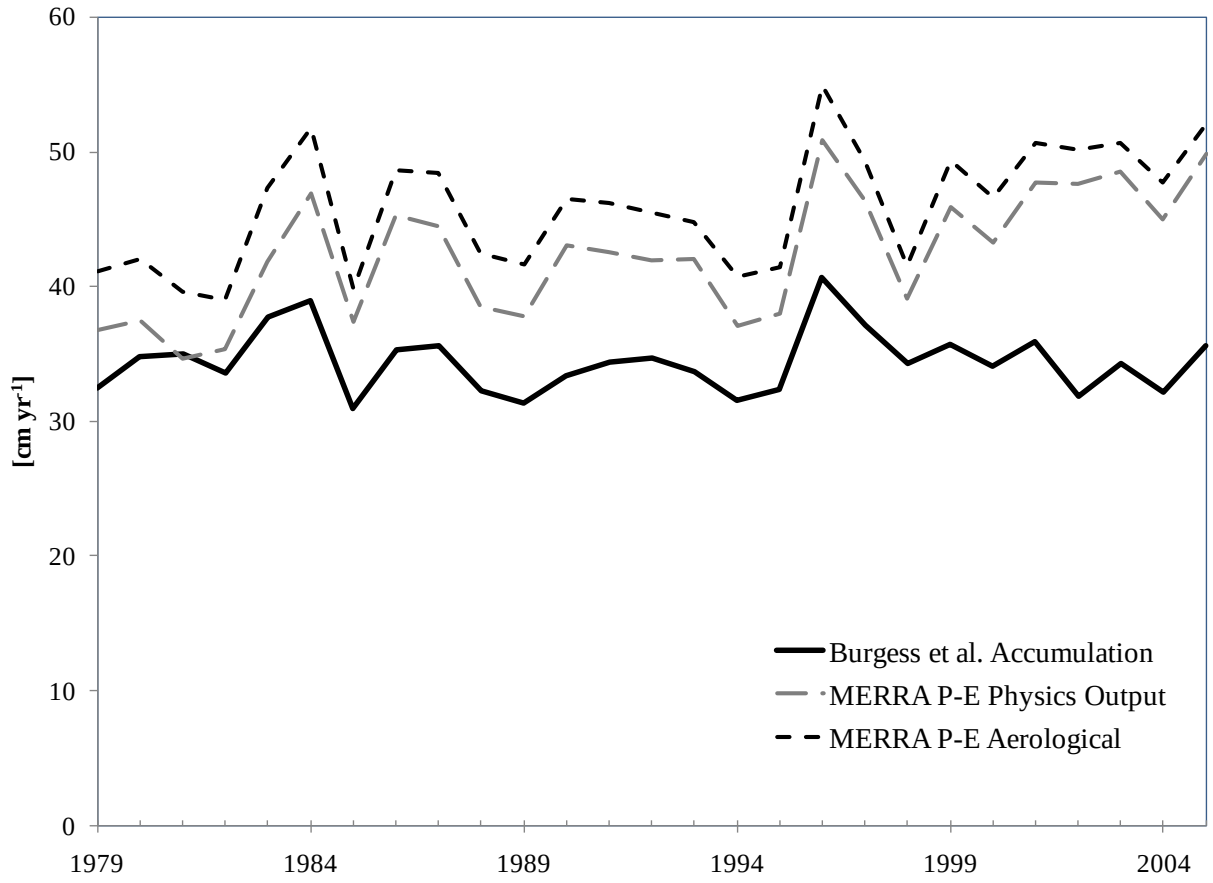

FIGURE 8. Comparison of MERRA with Greenland annual accumulation synthesis derived from data of Burgess et al. (2010), in cm yr^{-1}.

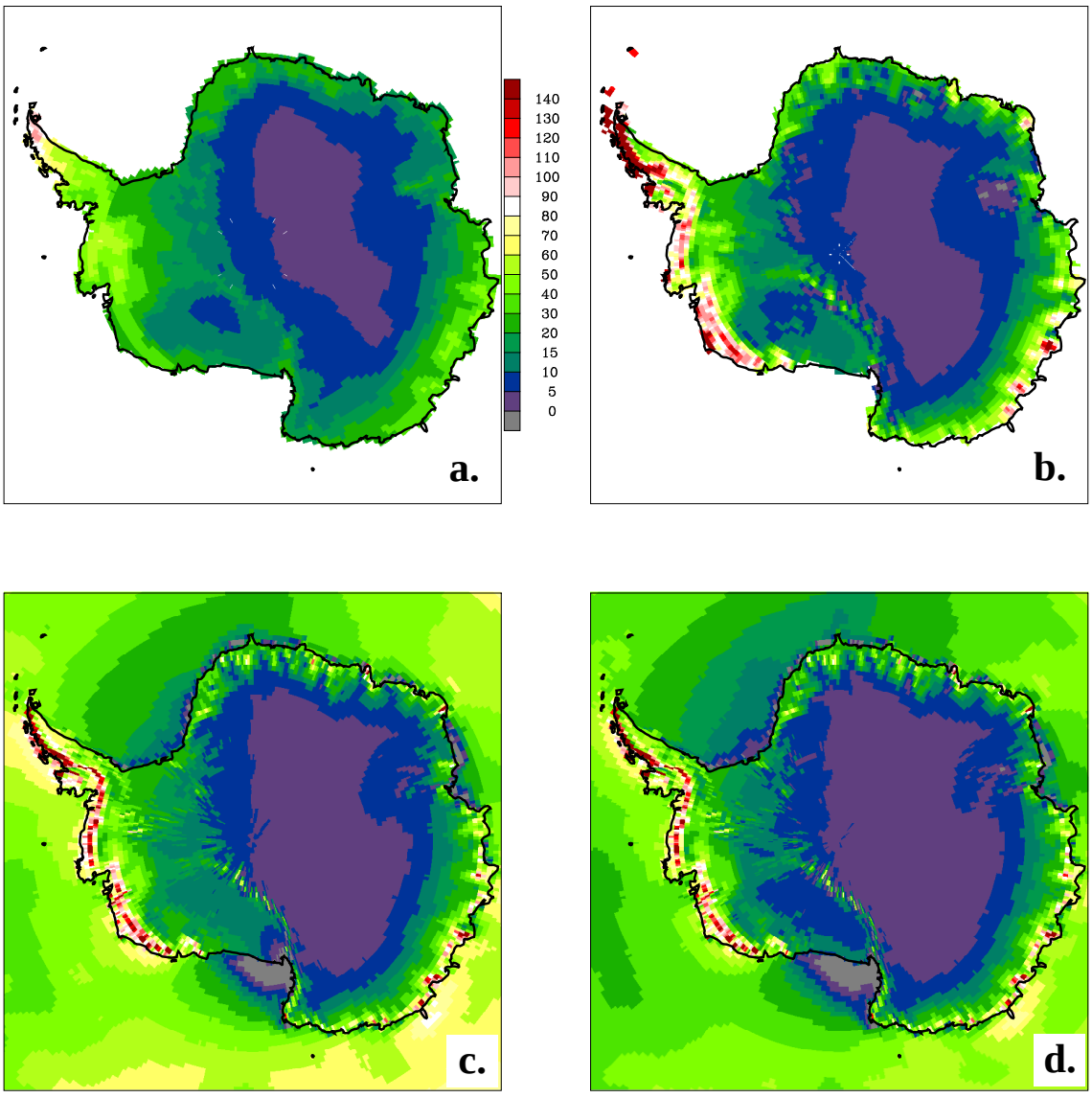

FIGURE 9. Grid cell shading of accumulation syntheses from (a.) Arthern et al. (2006) and (b.) van de Berg et al. (2006), (c.) MERRA 1979-2005 atmospheric moisture convergence, and (d.) MERRA 1979-2005 physics output $P-E$. All fields are shown at the native resolution of MERRA. The shading interval is every 5 cm yr^{-1} water-equivalent over the range 0 to 20 cm yr^{-1}, and every 10 cm yr^{-1} thereafter.